A&A 401, 43–56 (2003)
DOI: 10.1051/0004-6361:20021838

Astronomy & Astrophysics

The diffusion of radiation in moving media

IV. Flux vector, effective opacity, and expansion opacity

R. Wehrse[1,3], B. Baschek[1], and W. von Waldenfels[2,3]

[1] Institut für Theoretische Astrophysik, Tiergartenstrasse 15, 69121 Heidelberg, Germany
[2] Institut für Angewandte Mathematik, Im Neuenheimer Feld 294, 69120 Heidelberg, Germany
[3] Interdisziplinäres Zentrum für Wissenschaftliches Rechnen, Im Neuenheimer Feld 368, 69120 Heidelberg, Germany

Received 11 September 2002 / Accepted 10 December 2002

Abstract. For a given velocity and temperature field in a differentially moving 3D medium, the vector of the radiative flux is derived in the diffusion approximation. Due to the dependence of the velocity gradient on the direction, the associated effective opacity in general is a tensor. In the limit of small velocity gradients analytical expression are obtained which allow us to discuss the cases when the direction of the flux vector deviates from that of the temperature gradient. Furthermore the radiative flux is calculated for infinitely sharp, Poisson distributed spectral lines resulting in simple expressions that provide basic insight into the effect of the motions. In particular, it is shown how incomplete line lists affect the radiative flux as a function of the velocity gradient. Finally, the connection between our formalism and the concept of the expansion opacity introduced by Karp et al. (1977) is discussed.

Key words. diffusion – radiative transfer – stars: interiors – novae, cataclysmic variables – supernovae: general

1. Introduction

In this series on the effect of differential motions on the radiation in the diffusion limit, i.e. for optically thick media (Wehrse et al. 2000a,b, 2002), we have derived in Paper III the expectation values of radiative quantities, such as the flux and the radiative acceleration, for spectral lines which are *statistically* distributed according to the Poisson point process (cf. also Wehrse et al. 1998) and which have a finite intrinsic width. The stochastic description allowed us a general discussion of the effect of the differential motions in the medium on the radiation field in terms of the effective extinction coefficient.

This last paper of the series is devoted mainly to three topics: (i) the *vector* of the monochromatic and of the total radiative flux in 3D media, where the cases in which it deviates from the direction of the temperature gradient are of particular interest; (ii) the limiting case of *infinitely* sharp spectral lines whose profiles are described by Dirac δ functions, a useful approximation if the intrinsic widths are very small compared to the broadening by the motions. In particular Poisson distributed δ-lines have the advantage that many formulae can be integrated analytically and hence lead to relatively simple expressions for the expectation values of the radiative flux (whereas the more general expressions of Paper III frequently require involved numerical integrations); (iii) the connection between the concept of the *expansion* opacity by Karp et al. (1977) and our more general comoving-frame formalism which for stochastically distributed lines is expressed in terms of an *effective* opacity.

In Sect. 2 expressions for the flux vector in the diffusion limit are given for deterministic as well as for stochastic line extinction described by a Poisson point process, and the extinction coefficients associated to the different types of flux are introduced. Particularly simple expressions are obtained for the limit of small velocity gradients. The derivation of the vector of the radiative acceleration which is more involved than that of the flux is not treated here. In Sect. 3 the monochromatic flux is derived for the special case of infinitely sharp lines, described by Dirac δ-functions, again for deterministic as well as for stochastic line extinction. In particular the expectation value of the flux or, equivalently, the effective extinction are given for two specific line strength distributions of Poisson distributed δ-lines: for a power-law and for the case that all lines have equal strengths (Sect. 3.2.1). Furthermore, examples illustrating the effects of the motions, based on the assumption of infinitely sharp Poisson distributed lines, are given, and the limitations of the approximation by infinitely sharp lines are considered. In Sect. 4 we study the sensitivity of the flux to missing weak lines and show that it is a rather complicated function of the velocity gradient. In Sect. 5 we then discuss the connection of our comoving-frame scheme of the effective opacity based on Poisson distributed lines to the observer's-frame expansion opacity by Karp et al. and to selected comoving-frame expansion opacities used by other authors. Finally, Sect. 6 contains the conclusions of our results and an outlook.

Send offprint requests to: R. Wehrse,
e-mail: wehrse@ita.uni-heidelberg.de

References to equations of Papers I to III of this series are denoted by (I:n) to (III:m).

2. Vector of the radiative flux

As was shown in Paper I, the flux-like antisymmetric average $\mathcal{F}(s_0,\xi;w)$ (I:13) of the monochromatic specific intensities in the direction $\boldsymbol{n}$ at a spatial position s_0 and at a (logarithmic) wavelength ξ – here called "monochromatic flux" for short – serves as the basic "building block" for constructing radiative quantities such as the (monochromatic) flux vector by integration over all directions, and the total flux vector by integration over all wavelengths. $\boldsymbol{n} = \{n_i\}$ is a unit column vector which in cartesian coordinates reads $\boldsymbol{n} = \{n_x, n_y, n_z\} = \{\cos\varphi\sin\vartheta, \sin\varphi\sin\vartheta, \cos\vartheta\}$ where φ is the azimuthal and ϑ the polar angle.

The influence of a given velocity field $\boldsymbol{\beta}(\boldsymbol{x}) = \{\beta_i(x_k)\}$ on the radiation field in a *slowly* moving 3D medium is determined by the *"velocity gradient"*

$$w = \boldsymbol{n}\cdot\nabla(\boldsymbol{\beta}\cdot\boldsymbol{n}) = \boldsymbol{n}\frac{\partial\boldsymbol{\beta}}{\partial\boldsymbol{x}}\boldsymbol{n} = \sum_{i,j} n_i\frac{\partial\beta_i}{\partial x_j}n_j = \left\langle\boldsymbol{n}\middle|\frac{\partial\boldsymbol{\beta}}{\partial\boldsymbol{x}}\middle|\boldsymbol{n}\right\rangle \quad (1)$$

(I:33) which enters the comoving-frame radiative transfer equation for the monochromatic specific intensity in the direction $\boldsymbol{n}$ and hence $\mathcal{F}(s_0,\xi;w)$. In Eq. (1) $\partial\boldsymbol{\beta}/\partial\boldsymbol{x} = \{\partial\beta_i/\partial x_j\}$ is the Jacobian matrix of $\boldsymbol{\beta}$ (sometimes also called the vector gradient). In this paper we will furthermore apply the *bra-ket notation* of quantum mechanics (e.g. Cohen-Tanoudji 1977) which is particularly useful to indicate direct vector products, noting that $\langle\boldsymbol{n}| = \{n_i\}$, $|\boldsymbol{n}\rangle = \{n_i\}^{\mathrm{T}}$, $\langle\boldsymbol{n}|\boldsymbol{n}\rangle = \sum_i n_i^2 = 1$, and that $|\boldsymbol{n}\rangle\langle\boldsymbol{n}|$ is a tensor (matrix) with the dyadic products $n_i n_j$ as elements.

In the following we will first derive the flux vector for a deterministic line extinction coefficient, and subsequently give expressions for the corresponding expectation values for a stochastic description of the line distribution. In order to facilitate the use of the various symbols for the different types of flux and the associated extinction coefficients, we present a condensed overview in Table 1; the detailed relationships are summarized in Table A.1 of the appendix.

2.1. Flux vector for deterministic line extinction

In the *diffusion* approximation of the radiation field,

$$\mathcal{F}(s_0,\xi;w) = 2g(s_0,\xi,\boldsymbol{n})\Big[\chi_{\mathrm{n}}(\xi;w)\Big]^{-1} = 2\frac{\partial B(T,\xi)}{\partial T}\Big[\chi_{\mathrm{n}}(\xi;w)\Big]^{-1}\boldsymbol{n}\cdot\nabla T \quad (2)$$

holds, where the corresponding monochromatic extinction χ_{n} in the direction $\boldsymbol{n}$ for a differentially moving medium is given by

$$\Big[\chi_{\mathrm{n}}(\xi;w)\Big]^{-1} = \int_0^\infty \exp\left(-\frac{1}{w}\int_{\xi-ws}^{\xi}\chi(\zeta)\mathrm{d}\zeta\right)\mathrm{d}s \quad (3)$$

(I:6, 41). $B(T,\xi)$ is the Planck function at ξ for the temperature $T = T(s_0)$, and $\chi(\xi)$ is the "ordinary" static extinction coefficient (including the continuum) which for clarity we will denote in expressions for the flux in the static ($\lim w \to 0$) case by $\chi_0(\xi) \equiv \chi(\xi)$.

For the *static* case, $\chi_{\mathrm{n}}(\xi;w) \to \chi_0(\xi)$ so that the well-known conventional expression

$$\mathcal{F}(s_0,\xi) = 2g(s_0,\xi,\boldsymbol{n})\Big[\chi_0(\xi)\Big]^{-1} = 2\frac{\partial B(T,\xi)}{\partial T}\Big[\chi_0(\xi)\Big]^{-1}\boldsymbol{n}\cdot\nabla T \quad (4)$$

results.

The flux *vector*, obtained by integration of the directional fluxes over half the sphere (cf. I:12), can be written as

$$\boldsymbol{F}_w(s_0,\xi) = \int_{2\pi}\mathcal{F}(s_0,\xi;w)\,\boldsymbol{n}\,\mathrm{d}\omega = \frac{4\pi}{3}\frac{\partial B(T,\xi)}{\partial T}\Big[\boldsymbol{X}_\beta(\xi)\Big]^{-1}\nabla T \quad (5)$$

with the solid angle element $\mathrm{d}\omega = \mathrm{d}\varphi\sin\vartheta\mathrm{d}\vartheta$. After the integration over ω the flux vector no longer depends explicitly on the velocity gradient w; the subscript w of the flux vector only refers to the moving case and does not denote a variable. The extinction corresponding to $\boldsymbol{F}_w$ is

$$\Big[\boldsymbol{X}_\beta(\xi)\Big]^{-1} = \frac{3}{2\pi}\int_{2\pi}\Big[\chi_{\mathrm{n}}(\xi;w)\Big]^{-1}|\boldsymbol{n}\rangle\langle\boldsymbol{n}|\,\mathrm{d}\omega. \quad (6)$$

(The symbol $\boldsymbol{X}_\beta$ should not be confused with $X(\xi)$, the contribution of the lines to the extinction coefficient, cf. III:1.)

We point out that $w = w(\boldsymbol{n})$ is a scalar, but its value and hence that of χ_{n} are in general different in different directions $\boldsymbol{n}$. On the other hand the extinction coefficient $\boldsymbol{X}_\beta$ associated with the flux vector is a *tensor* or a matrix. Eq. (5) shows that the direction of $\boldsymbol{F}_w$ is determined by the vector $[\boldsymbol{X}_\beta]^{-1}\nabla T$ which in principle may differ in direction from the temperature gradient ∇T. This will be further elaborated to some extent for the limit of small velocity gradients in Sect. 2.2; one simple case where the directions of flux vector and temperature gradient diverge has already been discussed in Paper II (Sect. 5).

The static extinction coefficient χ_0 is independent of the direction $\boldsymbol{n}$, and the the *static* flux vector

$$\boldsymbol{F}(s_0,\xi) = \frac{4\pi}{3}\frac{\partial B(T,\xi)}{\partial T}\Big[\chi_0(\xi)\Big]^{-1}\nabla T \quad (7)$$

is always parallel to the temperature gradient.

By integration of (2) over all wavelengths we obtain the *total* flux in the direction $\boldsymbol{n}$,

$$\mathcal{F}_{\mathrm{tot}}(s_0;w) = \int_{-\infty}^{\infty}\mathcal{F}(s_0,\xi;w)\,\mathrm{e}^{\xi}\mathrm{d}\xi = 2\frac{\partial B(T)}{\partial T}\Big[\bar{\chi}_{\mathrm{n}}(w)\Big]^{-1}\boldsymbol{n}\cdot\nabla T \quad (8)$$

with $B(T)$ being the wavelength-integrated Planck function and

$$\Big[\bar{\chi}_{\mathrm{n}}(w)\Big]^{-1} = \int_{-\infty}^{\infty}G(s_0,\xi)\Big[\chi_{\mathrm{n}}(\xi;w)\Big]^{-1}\mathrm{d}\xi. \quad (9)$$

The weighting function (I:8)

$$G(s_0,\xi) = \left(\frac{\partial B(T,\xi)}{\partial T}\Big/\frac{\mathrm{d}B(T)}{\mathrm{d}T}\right)\mathrm{e}^{\xi} \quad (10)$$

Table 1. Overview of the notation for the various types of radiation flux in the diffusion approximation and their associated equivalent opacities.

	deterministic line list	stochastic line distribution (Poisson point process)
monochromatic		
flux in direction $\boldsymbol{n}$	$\mathcal{F}(s_0,\xi;w) \rightleftharpoons \left[\chi_{\rm n}(\xi;w)\right]^{-1}$	$\left\langle\mathcal{F}(s_0,\xi;w)\right\rangle \rightleftharpoons \left[\chi_{\rm eff,n}(\xi;w)\right]^{-1}$
– , *static*	$\mathcal{F}(s_0,\xi) \rightleftharpoons \left[\chi_0(\xi)\right]^{-1}$	$\left\langle\mathcal{F}(s_0,\xi)\right\rangle \rightleftharpoons \left[\chi_{\rm eff,0}(\xi)\right]^{-1}$
flux vector	$\boldsymbol{F}_w(s_0,\xi) \rightleftharpoons \left[\boldsymbol{X}_\beta(\xi)\right]^{-1}$	$\left\langle\boldsymbol{F}_w(s_0,\xi)\right\rangle \rightleftharpoons \left[\boldsymbol{X}_{\rm eff,\beta}(\xi)\right]^{-1}$
– , *static*	$\boldsymbol{F}(s_0,\xi) \rightleftharpoons \left[\chi_0(\xi)\right]^{-1}$	$\left\langle\boldsymbol{F}(s_0,\xi)\right\rangle \rightleftharpoons \left[\chi_{\rm eff,0}(\xi)\right]^{-1}$
wavelength-integrated		
flux in direction $\boldsymbol{n}$	$\mathcal{F}_{\rm tot}(s_0;w) \rightleftharpoons \left[\bar{\chi}_{\rm n}(w)\right]^{-1}$	$\left\langle\mathcal{F}_{\rm tot}(s_0;w)\right\rangle \rightleftharpoons \left[\bar{\chi}_{\rm eff,n}(w)\right]^{-1}$
– , *static*	$\mathcal{F}_{\rm tot}(s_0) \rightleftharpoons \left[\bar{\chi}_{\rm R}\right]^{-1}$	$\left\langle\mathcal{F}_{\rm tot}(s_0)\right\rangle \rightleftharpoons \left[\bar{\chi}_{\rm eff,0}\right]^{-1}$
flux vector	$\boldsymbol{F}_{{\rm tot},w}(s_0) \rightleftharpoons \left[\bar{\boldsymbol{X}}_\beta\right]^{-1}$	$\left\langle\boldsymbol{F}_{{\rm tot},w}(s_0)\right\rangle \rightleftharpoons \left[\bar{\boldsymbol{X}}_{\rm eff,\beta}\right]^{-1}$
– , *static*	$\boldsymbol{F}_{\rm tot}(s_0) \rightleftharpoons \left[\bar{\chi}_{\rm R}\right]^{-1}$	$\left\langle\boldsymbol{F}_{\rm tot}(s_0)\right\rangle \rightleftharpoons \left[\bar{\chi}_{\rm eff,0}\right]^{-1}$

is isotropic, i.e. independent of the direction $\boldsymbol{n}$.

The *total flux vector* is given by

$$\begin{aligned}\boldsymbol{F}_{{\rm tot},w}(s_0) &= \int_{-\infty}^{\infty} \boldsymbol{F}_{{\rm tot},w}(s_0,\xi)\,{\rm e}^{\xi}{\rm d}\xi \\ &= \frac{4\pi}{3}\,\frac{\partial B(T)}{\partial T}\left[\bar{\boldsymbol{X}}_\beta\right]^{-1}\nabla T \end{aligned} \tag{11}$$

with

$$\left[\bar{\boldsymbol{X}}_\beta\right]^{-1} = \int_{-\infty}^{\infty} G(s_0,\xi)\left[\boldsymbol{X}_\beta(\xi)\right]^{-1}{\rm d}\xi. \tag{12}$$

As for the monochromatic flux vector (5), also the direction of the total flux vector may differ from that of ∇T, albeit in a different way, determined by the tensor $\bar{\boldsymbol{X}}_\beta$.

The *static* expressions for the total directional flux and flux vector are

$$\mathcal{F}_{\rm tot}(s_0) = 2\,\frac{\partial B(T)}{\partial T}\left[\bar{\chi}_{\rm R}\right]^{-1}\boldsymbol{n}\cdot\nabla T, \tag{13}$$

$$\boldsymbol{F}_{\rm tot}(s_0) = \frac{4\pi}{3}\,\frac{\partial B(T)}{\partial T}\left[\bar{\chi}_{\rm R}\right]^{-1}\nabla T, \tag{14}$$

where $\bar{\chi}_{\rm R} = \bar{\chi}_{\rm R}(s_0)$ is the conventional *Rosseland* opacity, i.e.

$$\left[\bar{\chi}_{\rm R}\right]^{-1} = \int_{-\infty}^{\infty} G(s_0,\xi)\left[\chi_0(\xi)\right]^{-1}{\rm d}\xi. \tag{15}$$

2.2. Deterministic flux vector for the limit of small velocity gradients

Expansion of the flux in the direction $\boldsymbol{n}$ to second order in terms of $w = \langle\boldsymbol{n}|\partial\boldsymbol{\beta}/\partial\boldsymbol{x}|\boldsymbol{n}\rangle$ (Eq. (1)) with the static case as reference value yields

$$\begin{aligned}\mathcal{F}(s_0,\xi;w) &= \left[\frac{\chi_{\rm n}(\xi;w)}{\chi_0(\xi)}\right]^{-1}\mathcal{F}(s_0,\xi) \\ &= \left[1 + f_1(\xi)\left\langle\boldsymbol{n}\right|\frac{\partial\boldsymbol{\beta}}{\partial\boldsymbol{x}}\left|\boldsymbol{n}\right\rangle + \frac{1}{2}f_2(\xi)\left(\left\langle\boldsymbol{n}\right|\frac{\partial\boldsymbol{\beta}}{\partial\boldsymbol{x}}\left|\boldsymbol{n}\right\rangle\right)^2\right]\mathcal{F}(s_0,\xi)\end{aligned} \tag{16}$$

where

$$f_1(\xi) = -\frac{\partial}{\partial\xi}\frac{1}{\chi_0(\xi)}, \quad f_2(\xi) = +\frac{\partial^2}{\partial\xi^2}\frac{1}{\chi_0(\xi)^2} \tag{17}$$

according to Eq. (II:17). Note that the additional dependence of f_1 and f_2 on s_0 is not explicitly denoted here.

In order to derive the monochromatic flux vector from Eqs. (5) and (6), we utilize the bra-ket formalism for the further evaluation, noting that $\int_{2\pi}|\boldsymbol{n}\rangle\langle\boldsymbol{n}|{\rm d}\omega = 2\pi/3\,\boldsymbol{E}$, and get

$$\begin{aligned}\boldsymbol{F}_w(s_0,\xi) &= \left[\frac{\boldsymbol{X}_\beta(\xi)}{\chi_0(\xi)}\right]^{-1}\boldsymbol{F}(s_0,\xi) \\ &= \left[\boldsymbol{E} + \frac{3}{2\pi}f_1(\xi)\int_{2\pi}|\boldsymbol{n}\rangle\langle\boldsymbol{n}|\frac{\partial\boldsymbol{\beta}}{\partial\boldsymbol{x}}|\boldsymbol{n}\rangle\langle\boldsymbol{n}|{\rm d}\omega\right. \\ &\quad \left. + \frac{3}{4\pi}f_2(\xi)\int_{2\pi}|\boldsymbol{n}\rangle\langle\boldsymbol{n}|\left(\frac{\partial\boldsymbol{\beta}}{\partial\boldsymbol{x}}|\boldsymbol{n}\rangle\langle\boldsymbol{n}|\right)^2{\rm d}\omega\right]\boldsymbol{F}(s_0,\xi)\end{aligned} \tag{18}$$

with $\boldsymbol{E}$ being the unit matrix.

If we represent the Jacobian matrix as a sum of a symmetric (s) and an antisymmetric (a) matrix,

$$\frac{\partial\boldsymbol{\beta}}{\partial\boldsymbol{x}} = \left(\frac{\partial\boldsymbol{\beta}}{\partial\boldsymbol{x}}\right)_{\rm s} + \left(\frac{\partial\boldsymbol{\beta}}{\partial\boldsymbol{x}}\right)_{\rm a} \tag{19}$$

with

$$\left(\frac{\partial\boldsymbol{\beta}}{\partial\boldsymbol{x}}\right)_{\rm s} = \frac{1}{2}\left[\left(\frac{\partial\boldsymbol{\beta}}{\partial\boldsymbol{x}}\right) + \left(\frac{\partial\boldsymbol{\beta}}{\partial\boldsymbol{x}}\right)^{\rm T}\right], \tag{20}$$

we find that the *anti*symmetric matrix does *not* contribute to the integral in Eq. (18) due to the *even* number of $\boldsymbol{n}$ terms. Since a straightforward angle-integration, e.g. with Mathematica or Maple, results in expressions that allow us only little insight, we extend the integrals in Eq. (18) to the whole sphere so that the problem becomes rotationally invariant (cf. e.g. Weil 1966). Therefore only the symmetric part of the Jacobian matrix $(\partial\boldsymbol{\beta}/\partial\boldsymbol{x})_{\rm s}$, its square $(\partial\boldsymbol{\beta}/\partial\boldsymbol{x})_{\rm s}^2$, and their traces can appear. After some lengthy algebra we obtain

$$\boldsymbol{F}_w(s_0,\xi) = \left[\boldsymbol{E} + \frac{1}{5}f_1(\xi)\,\boldsymbol{\Psi_1} + \frac{1}{70}f_2(\xi)\,\boldsymbol{\Psi_2}\right]\boldsymbol{F}(s_0,\xi) \tag{21}$$

with the matrices

$$\boldsymbol{\Psi_1} = {\rm Tr}\left(\frac{\partial\boldsymbol{\beta}}{\partial\boldsymbol{x}}\right)_{\rm s}\boldsymbol{E} + \left(\frac{\partial\boldsymbol{\beta}}{\partial\boldsymbol{x}}\right)_{\rm s} \tag{22}$$

and

$$\mathbf{\Psi_2} = \left(\mathrm{Tr}\left(\frac{\partial \boldsymbol{\beta}}{\partial \boldsymbol{x}}\right)_\mathrm{s}\right)^2 \boldsymbol{E} + 2\,\mathrm{Tr}\left(\frac{\partial \boldsymbol{\beta}}{\partial \boldsymbol{x}}\right)_\mathrm{s}^2 \boldsymbol{E} + 4\,\mathrm{Tr}\left(\frac{\partial \boldsymbol{\beta}}{\partial \boldsymbol{x}}\right)_\mathrm{s}\left(\frac{\partial \boldsymbol{\beta}}{\partial \boldsymbol{x}}\right)_\mathrm{s} + 8\left(\frac{\partial \boldsymbol{\beta}}{\partial \boldsymbol{x}}\right)_\mathrm{s}^2 \tag{23}$$

which are functions of the Jacobian matrix $\partial\boldsymbol{\beta}/\partial\boldsymbol{x}$. Analogously we derive for the *wavelength-integrated* directional flux

$$\begin{aligned}\mathcal{F}_\mathrm{tot}(s_0; w) &= \left[\frac{\bar{\chi}_\mathrm{n}(w)}{\bar{\chi}_\mathrm{R}}\right]^{-1} \mathcal{F}_\mathrm{tot}(s_0) \qquad (24)\\ &= \left[1 + \hat{\eta}_1(s_0)\langle \boldsymbol{n}|\frac{\partial \boldsymbol{\beta}}{\partial \boldsymbol{x}}|\boldsymbol{n}\rangle + \frac{1}{2}\hat{\eta}_2(s_0)\left(\left\langle \boldsymbol{n}\middle|\frac{\partial \boldsymbol{\beta}}{\partial \boldsymbol{x}}\middle|\boldsymbol{n}\right\rangle\right)^2\right]\mathcal{F}_\mathrm{tot}(s_0)\end{aligned}$$

with the coefficients (cf. also II:20, 21)

$$\hat{\eta}_k(s_0) = \int_{-\infty}^{\infty} G(s_0, \xi)\left[\frac{\chi_0(\xi)}{\bar{\chi}_\mathrm{R}}\right]^{-1} f_k(\xi)\,\mathrm{d}\xi \tag{25}$$

($k = 1, 2$). Note that $\hat{\eta}_1 = \eta_1$, but $\hat{\eta}_2 = 2\eta_2$, where the η_k are the corresponding coefficients entering (II:18).

The vector of the total flux is

$$\begin{aligned}\boldsymbol{F}_{\mathrm{tot},w}(s_0) &= \left[\frac{\bar{\boldsymbol{X}}_\beta}{\bar{\chi}_\mathrm{R}}\right]^{-1} \boldsymbol{F}_\mathrm{tot}(s_0)\\ &= \left[\boldsymbol{E} + \frac{1}{5}\hat{\eta}_1(s_0)\mathbf{\Psi_1} + \frac{1}{70}\hat{\eta}_2(s_0)\mathbf{\Psi_2}\right]\boldsymbol{F}_\mathrm{tot}(s_0). \qquad (26)\end{aligned}$$

Since often $\hat{\eta}_1 = 0$ and $\hat{\eta}_2 < 0$ (see Papers II and III), the above expressions for the flux vectors show that spectral lines reduce the absolute value of the flux vector. The unit matrices in Eq. (23) indicate that this may happen even in cases when there is no Doppler effect in the direction of the flux vector.

In a general velocity field there is shearing and therefore the Jacobian matrix contains off-diagonal elements. It is seen that in this case the flux vector need not point into the direction of the temperature gradient. Equation (26), however, has been derived for a *given* velocity field, but any difference between the directions of flux vector and temperature gradient will lead to a rearrangement of the temperature and velocity patterns in the medium. It should furthermore be kept in mind that in this series we neglect aberration and advection (cf. I:25, 33) which also influence the orientation of the flux vector. However, we expect these effects to be much smaller than those caused by the Doppler effects discussed here.

In radiation hydrodynamics a further important quantity is the *divergence* of the total flux vector which enters the local radiative energy balance. For small velocity gradients it reads

$$\begin{aligned}\nabla\cdot\boldsymbol{F}_{\mathrm{tot},w}(s_0) &= \nabla\cdot\boldsymbol{F}_\mathrm{tot}(s_0)\\ &+ \frac{1}{5}\nabla\hat{\eta}_1(s_0)\cdot\left(\mathbf{\Psi_1}\boldsymbol{F}_\mathrm{tot}(s_0)\right) + \frac{1}{5}\hat{\eta}_1(s_0)\nabla\cdot\left(\mathbf{\Psi_1}\boldsymbol{F}_\mathrm{tot}(s_0)\right)\\ &+ \frac{1}{70}\nabla\hat{\eta}_2(s_0)\cdot\left(\mathbf{\Psi_2}\boldsymbol{F}_\mathrm{tot}(s_0)\right) + \frac{1}{70}\hat{\eta}_2(s_0)\nabla\cdot\left(\mathbf{\Psi_2}\boldsymbol{F}_\mathrm{tot}(s_0)\right). \qquad (27)\end{aligned}$$

Note that div $\boldsymbol{F}_{\mathrm{tot},w}$ depends on the divergence of the correction vector and on spatial gradient of the coefficients $\hat{\eta}_k$.

2.3. Flux vector for a stochastic line distribution

Frequently it is advantageous to apply a *stochastic* line distribution, e.g. based on the Poisson point process (cf. Wehrse et al. 1998 and Paper III), so that we also require the *expectation values*, denoted by acute brackets, of the various types of flux and their corresponding *effective* extinction coefficients. Since the general structure of these expressions is completely analogous to that of the deterministic ones (Sect. 2.1), it suffices in many cases to refer to the overview of the nomenclature of the fluxes and their corresponding extinction coefficients in Table 1 in order to write down their relationships explicitly.

In the following we assume that the spectral lines are distributed according to a *Poisson point process*. As was discussed in Paper III, then the expectation values of all radiative quantities are functionals of the two *basic* functions, the line extinction coefficient $\chi(\xi, \vartheta, \xi - \hat{\xi})$ and the line density $\varrho(\hat{\xi}, \vartheta)$. In addition they depend on the velocity gradient $|w|$, the temperature gradient ∇T, and the continuous extinction $\chi_\mathrm{c}(\xi)$ which is assumed to be a slowly varying function of ξ. The (logarithmic) wavelength ξ, the line position $\hat{\xi}$, and the line parameter ϑ (comprising strength and intrinsic width) are regarded as continuous variables. For further details, in particular for the derivation of the expectation values, see Paper III.

For *Poisson distributed* lines the expectation value of the monochromatic flux (cf. Eqs. (III:10), (20), (21)) is

$$\left\langle \mathcal{F}(s_0, \xi; w)\right\rangle = 2\,\frac{\partial B(T,\xi)}{\partial T}\left[\chi_\mathrm{eff,n}(\xi; w)\right]^{-1} \boldsymbol{n}\cdot\nabla T \tag{28}$$

with

$$\begin{aligned}\left[\chi_\mathrm{eff,n}(\xi; w)\right]^{-1} &= \int_0^\infty \mathrm{e}^{-\chi_\mathrm{c} s}\exp\left[\int_\Theta\int_{-\infty}^{\infty}\varrho(\hat{\xi},\vartheta)\right.\\ &\left.\times\left\{\exp\left(-\frac{1}{w}\int_{\xi-ws}^{\xi}\chi(\hat{\xi},\vartheta,\zeta-\hat{\xi})\mathrm{d}\zeta\right) - 1\right\}\mathrm{d}\hat{\xi}\,d\vartheta\right]\mathrm{d}s. \qquad (29)\end{aligned}$$

Its static limit is

$$\left\langle \mathcal{F}(s_0, \xi)\right\rangle = 2\,\frac{\partial B(T,\xi)}{\partial T}\left[\chi_\mathrm{eff,0}(\xi)\right]^{-1} \boldsymbol{n}\cdot\nabla T \tag{30}$$

with the associated effective extinction

$$\left[\chi_\mathrm{eff,0}(\xi)\right]^{-1} = \int_0^\infty \mathrm{e}^{-\chi_\mathrm{c} s}\Omega_0(\xi, s)\,\mathrm{d}s \tag{31}$$

which – as $\chi_0(\xi)$ – is independent of the direction $\boldsymbol{n}$. Here the abbreviation (III:11, 42)

$$\Omega_0(\xi, s) = \exp\left(\int_\Theta\int_{-\infty}^{\infty}\varrho(\hat{\xi},\vartheta)\left\{\mathrm{e}^{-\chi(\hat{\xi},\vartheta,\xi-\hat{\xi})\cdot s} - 1\right\}\mathrm{d}\hat{\xi}\mathrm{d}\vartheta\right) \tag{32}$$

has been used. We note that in (III:20) the simplified notation χ_eff had been introduced instead of $\chi_\mathrm{eff,n}$.

Analogously to Eq. (16) we may express the expectation value of the flux in term of its static value, i.e.

$$\left\langle \mathcal{F}(s_0, \xi; w)\right\rangle = \left[\frac{\chi_\mathrm{eff,n}(\xi; w)}{\chi_\mathrm{eff,0}(\xi)}\right]^{-1}\left\langle \mathcal{F}(s_0, \xi)\right\rangle, \tag{33}$$

with $\chi_\mathrm{eff,n}/\chi_\mathrm{eff,0} \geq 1$ presenting a measure of the effect of the motions. Then for the expectation value of the flux vector

$$\left\langle \boldsymbol{F}_w(s_0, \xi)\right\rangle = \left[\frac{\boldsymbol{X}_{\mathrm{eff},\beta}(\xi)}{\chi_\mathrm{eff,0}(\xi)}\right]^{-1}\left\langle \boldsymbol{F}(s_0, \xi)\right\rangle \tag{34}$$

holds (cf. Eqs. (5), (7)), where the monochromatic effective extinction tensor $\boldsymbol{X}_{\mathrm{eff},\beta}(\xi)$ can be obtained from $\chi_{\mathrm{eff,n}}(\xi; w)$ as in the deterministic case (cf. Eq. (6)).

The expectation values of the wavelength-integrated mean extinctions (9), (12), and (15) can be calculated by

$$\left[\bar{\chi}_{\mathrm{eff,n}}(w)\right]^{-1} = \int_{-\infty}^{\infty} G(s_0,\xi)\left[\chi_{\mathrm{eff,n}}(\xi; w)\right]^{-1} \mathrm{d}\xi \tag{35}$$

$$\left[\bar{\boldsymbol{X}}_{\mathrm{eff},\beta}\right]^{-1} = \int_{-\infty}^{\infty} G(s_0,\xi)\left[\boldsymbol{X}_{\mathrm{eff},\beta}(\xi)\right]^{-1} \mathrm{d}\xi \tag{36}$$

$$\left[\bar{\chi}_{\mathrm{eff},0}\right]^{-1} = \int_{-\infty}^{\infty} G(s_0,\xi)\left[\chi_{\mathrm{eff},0}(\xi)\right]^{-1} \mathrm{d}\xi. \tag{37}$$

2.4. Stochastic flux vector for the limit of small velocity gradients

For small velocity gradients $w = \langle \boldsymbol{n}|\partial\boldsymbol{\beta}/\partial\boldsymbol{x}|\boldsymbol{n}\rangle$ we use the results of Sect. 5.2 of paper III upon the assumption that the line density $\varrho(\hat{\xi},\vartheta)$ varies sufficiently slowly with $\hat{\xi}$. Then the first-order term in w vanishes, and only the coefficient

$$\omega_2(\xi, s) = -\frac{s^4}{12}\int_\Theta \int_{-\infty}^{\infty} \varrho(\hat{\xi},\vartheta) \times\left(\frac{\partial\chi(\hat{\xi},\vartheta,\xi-\hat{\xi})}{\partial\xi}\right)^2 \mathrm{e}^{-\chi(\hat{\xi},\vartheta,\xi-\hat{\xi})\cdot s}\mathrm{d}\hat{\xi}\mathrm{d}\vartheta \tag{38}$$

(III:46, 15) is required for the calculation of the monochromatic expectation values so that

$$\left\langle \mathcal{F}(s_0,\xi; w)\right\rangle = \left[1 + \frac{1}{2}\, f_2^*(\xi)\, w^2\right]\left\langle \mathcal{F}(s_0,\xi)\right\rangle \tag{39}$$

and

$$\left\langle \boldsymbol{F}_w(s_0,\xi)\right\rangle = \left[\boldsymbol{E} + \frac{1}{70}\, f_2^*(\xi)\, \boldsymbol{\Psi}_2\right]\left\langle \boldsymbol{F}(s_0,\xi)\right\rangle \tag{40}$$

with

$$f_2^*(\xi) = \frac{\int_0^\infty \mathrm{e}^{-\chi_c(\xi)s}\, \Omega_0(\xi, s)\cdot\omega_2(\xi, s)\,\mathrm{d}s}{\int_0^\infty \mathrm{e}^{-\chi_c(\xi)s}\, \Omega_0(\xi, s)\,\mathrm{d}s}. \tag{41}$$

The expectation values of the corresponding wavelength-integrated expressions are given by

$$\left\langle \mathcal{F}_{\mathrm{tot}}(s_0; w)\right\rangle = \left[1 + \frac{1}{2}\,\hat{\eta}_2^*(s_0)\, w^2\right]\left\langle \mathcal{F}_{\mathrm{tot}}(s_0)\right\rangle, \tag{42}$$

$$\left\langle \boldsymbol{F}_{\mathrm{tot},w}(s_0)\right\rangle = \left[\boldsymbol{E} + \frac{1}{70}\hat{\eta}_2^*(s_0)\, \boldsymbol{\Psi}_2\right]\left\langle \boldsymbol{F}_{\mathrm{tot}}(s_0)\right\rangle \tag{43}$$

with

$$\hat{\eta}_2^*(s_0) = \frac{\int_{-\infty}^{\infty}\int_0^\infty G(s_0,\xi)\,\mathrm{e}^{-\chi_c(\xi)s}\,\Omega_0(\xi, s)\cdot\omega_2(\xi, s)\,\mathrm{d}s\,\mathrm{d}\xi}{\int_{-\infty}^{\infty}\int_0^\infty G(s_0,\xi)\,\mathrm{e}^{-\chi_c(\xi)s}\,\Omega_0(\xi, s)\,\mathrm{d}s\,\mathrm{d}\xi}. \tag{44}$$

Note that $\hat{\eta}_2^* = 2\eta_2^*$, with η_2^* being defined by (III:56). Since $\omega_2 < 0$ and G as well as Ω_0 are positive functions, $\hat{\eta}_2^*$ is always negative.

For small velocity gradients the *divergence* of the expectation value of the total flux is

$$\nabla\cdot\left\langle \boldsymbol{F}_{\mathrm{tot},w}(s_0)\right\rangle = \nabla\cdot\left\langle \boldsymbol{F}_{\mathrm{tot}}(s_0)\right\rangle + \frac{1}{70}\nabla\hat{\eta}_2^*(s_0)\cdot\left(\boldsymbol{\Psi}_2\left\langle \boldsymbol{F}_{\mathrm{tot}}(s_0)\right\rangle\right) + \frac{1}{70}\,\hat{\eta}_2^*(s_0)\,\nabla\cdot\left(\boldsymbol{\Psi}_2\left\langle \boldsymbol{F}_{\mathrm{tot}}(s_0)\right\rangle\right), \tag{45}$$

where – analogously to the deterministic case – also the gradient of the coefficient $\hat{\eta}_2^*$ enters.

3. Infinitely narrow spectral lines

Throughout this and the following section we assume infinitely sharp line profiles, presented by a *Dirac δ-function*, so that the contribution of each line l at position $\hat{\xi}_l$ to the line extinction coefficient (II:8) reads

$$\chi_l(\xi) = A_l \cdot \delta(\xi - \hat{\xi}_l). \tag{46}$$

3.1. Single infinitely narrow lines

For the study of a *single* infinitely narrow line on the continuum χ_c we have to return to Eq. (I:39) and find for the flux

$$\mathcal{F}(s_o,\xi; w) = 2\,\frac{\partial B(T,\xi)}{\partial T}\,\boldsymbol{n}\cdot\nabla T \times\frac{1}{\chi_c(\xi)}\cdot\begin{cases}\left[1 - \mathrm{e}^{-\chi_c(\xi)\cdot(\xi-\hat{\xi})/w}\left(1 - \mathrm{e}^{-A/w}\right)\right] & \text{for } \xi > \hat{\xi}\\ 1 & \xi < \hat{\xi}\end{cases}. \tag{47}$$

This expression behaves perfectly well for small $|w|$, but it turns out that – in contrast to the case of lines of finite width – there is no sensible Taylor series illustrating the flux dependence since all derivatives of the function $\exp(-A/w)$ are identically zero for $w = 0$ (cf. Fichtenholz 1973, for a discussion of the analytical properties of the function $\exp(-1/x^2)$).

The ξ-dependence of the flux corresponding to a sequence of narrowing Lorentz line profiles is shown in Fig. 1. It is seen that for the parameters used the wavelength dependence of $\mathcal{F}$ is fully determined by the intrinsic line width for about $\gamma \geq w$, and that the influence ceases for $\gamma \leq w$. Note also that the short-wavelength wing gets steeper and steeper for decreasing γ. For increasing velocity gradients (Fig. 2) the wavelength range of influence of a line gets larger and larger as expected but the minimum flux is increased.

The typical shape of the profiles in Figs. 1 and 2 agrees *qualitatively* with that of the effective expansion opacity in Fig. 1 of Karp et al. (1977) if it is taken into account that we plot the flux instead of the opacity and prefer a logarithmic wavelength scale instead of a frequency scale.

3.2. Flux and effective opacity for Poisson distributed infinitely sharp lines

For Poisson distributed infinitely sharp lines the line extinction coefficient (III:7) becomes

$$\chi(\hat{\xi},\vartheta,\xi-\hat{\xi}) = A\cdot\delta(\xi - \hat{\xi}), \tag{48}$$

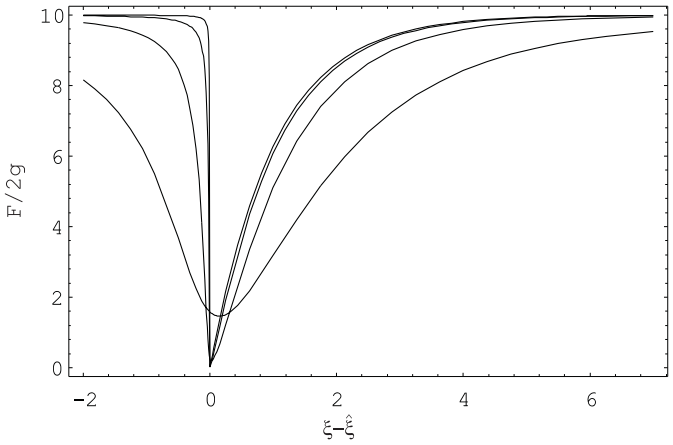

Fig. 1. Flux distributions $\mathcal{F}(s_0, \xi; w)$ of individual narrow *Lorentz* lines with A and χ_c kept constant. The curves refer to different damping constants γ.

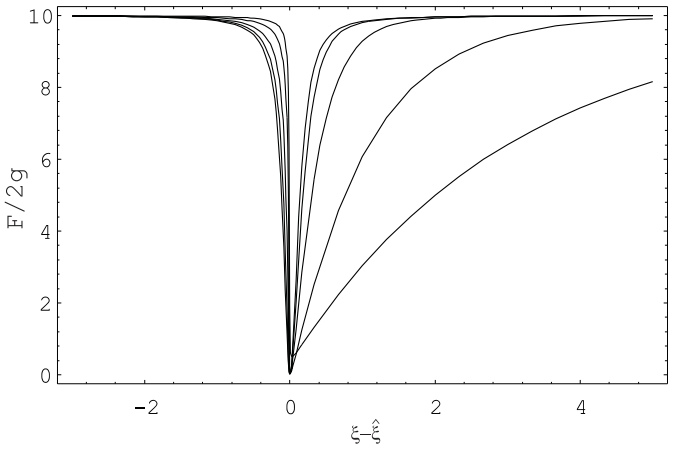

Fig. 2. Flux distributions $\mathcal{F}(s_0, \xi; w)$ of individual *infinitely* narrow lines with A and χ_c kept constant. The curves refer to different velocity gradients w.

where the line shape parameter ϑ is reduced to the line strength A, and ξ, the line position $\hat{\xi}$, and A are regarded as continuous variables.

We assume that the *line density* can be written as

$$\varrho(\hat{\xi}, \vartheta) = \varrho(\xi, A) = \varrho(\xi) \cdot f(A) \tag{49}$$

where $\varrho(\xi)$ is the number of lines at the position ξ in a unit logarithmic wavelength interval $\Delta\xi = \Delta \ln \xi = 1$ and $f(A)$ – normalized according to $\int_A f(A)\mathrm{d}A = 1$ – is the distribution of the line strengths which we assume to be independent of ξ. For the discussion of examples it will turn out useful to characterize the strength distribution primarily by its first moment, the *mean line strength*

$$\bar{A} = \int_A A f(A)\mathrm{d}A, \tag{50}$$

and furthermore to write the total extinction due to *all* lines in a unit ξ-interval at the position ξ as $\chi_{\mathrm{line}}(\xi) = \varrho(\xi)\,\bar{A}$, or, relative to the continuous extinction in the same ξ-interval, as

$$\Lambda(\xi) = \frac{\chi_{\mathrm{line}}(\xi)}{\chi_c(\xi)} = \frac{\varrho(\xi)\,\bar{A}}{\chi_c(\xi)} = \varrho(\xi) \cdot \frac{\bar{A}}{|w|} \cdot \frac{|w|}{\chi_c(\xi)}. \tag{51}$$

In order to elucidate the physical significance of the parameter combinations $|w|/\chi_c$ and $|w|/\bar{A}$, we introduce the differentials of the optical thickness in the continuum, $\mathrm{d}\tau_c = \chi_c\,\mathrm{d}s$, and in an "average" line $\mathrm{d}\tau_{\mathrm{line}} = \chi_{\mathrm{line}}\,\mathrm{d}s$, and, expressing the velocity by its gradient $\mathrm{d}\beta = \mathrm{d}v/c = w\,\mathrm{d}s$, we yield

$$\frac{\mathrm{d}\beta}{\mathrm{d}\tau_c} = \frac{|w|}{\chi_c(\xi)}, \qquad \frac{\mathrm{d}\beta}{\mathrm{d}\tau_{\mathrm{line}}} = \frac{|w|}{\varrho(\xi)\bar{A}}. \tag{52}$$

$|w|/\chi_c$ is thus the Doppler spread (in logarithmic wavelength units) $|\mathrm{d}\xi_{D,c}|$ over the mean free path $1/\chi_c(\xi)$ of a photon in the continuum, and $|w|/\bar{A}$ is the line density $\varrho(\xi)$ times the velocity change $|\mathrm{d}\xi_{D,\mathrm{line}}|$ over one mean free path of a photon in an "average" spectral line.

The expectation value of the line contribution to the *extinction coefficient* for *Poisson distributed*, infinitely sharp lines has already been calculated by Wehrse et al. (1998). For the diffusion approximation, their simple result allows us to perform the integration over s analytically yielding for the monochromatic flux $\langle\mathcal{F}(s_0, \xi; w)\rangle$ (28) or, equivalently, the effective monochromatic extinction (29)

$$\begin{aligned}\chi_{\mathrm{eff,n}}(\xi; w) &= \left[\int_0^\infty \mathrm{e}^{-\chi_c(\xi)s} \right.\\ &\quad \left. \times \exp\left(|w|\,\varrho(\xi)\int_A f(A)\left\{\mathrm{e}^{-A/|w|} - 1\right\}\mathrm{d}A \cdot s\right)\mathrm{d}s\right]^{-1}\\ &= \chi_c(\xi) + |w|\,\varrho(\xi)\int_A f(A)\left\{1 - \mathrm{e}^{-A/|w|}\right\}\mathrm{d}A. \end{aligned}\tag{53}$$

For the *static* case ($w \to 0$), $\chi_{\mathrm{eff,n}}(\xi; w)$ reduces to

$$\chi_{\mathrm{eff},0}(\xi) = \chi_c(\xi) \tag{54}$$

so that we regain the the familiar result that infinitely sharp lines do not at all contribute to the conventional (static) Rosseland opacity.

The effect of the motions in the case of Poisson distributed, infinitely narrow lines is thus described by

$$\begin{aligned}\left.\frac{\chi_{\mathrm{eff,n}}(\xi; w)}{\chi_{\mathrm{eff},0}(\xi)}\right|_\delta &= 1 + \frac{|w|\,\varrho(\xi)}{\chi_c(\xi)}\int_A f(A)\left\{1 - \mathrm{e}^{-A/|w|}\right\}\mathrm{d}A\\ &= 1 + \frac{\Lambda(\xi)}{\bar{A}/|w|}\int_A f(A)\left\{1 - \mathrm{e}^{-A/|w|}\right\}\mathrm{d}A \end{aligned}\tag{55}$$

(cf. Eq. (33)) and depends on the parameter $\Lambda = \varrho\bar{A}/\chi_c$ and the parameters describing the density distribution $f(A)$ including $\bar{A}$.

Concerning the extinction coefficient $\boldsymbol{X}_{\mathrm{eff},\beta}$ and the expectation value of the flux *vector* $\langle \boldsymbol{F}_w \rangle$ associated with it, we cannot give convenient expressions since integrals of type $\int \sin^i x \cos^j x \exp(-1/(\sin^l x \cos^m x))\mathrm{d}x$ with $i, j, l, m \geq 1$ being integers (cf. Eq. (55)) cannot be expressed analytically in a closed form and since there is no power law expansion of the directional flux for infinitely narrow lines (see Sect. 3.1). However, we note that qualitatively the factorization into a velocity-dependent part and a frequency-dependent part should be conserved.

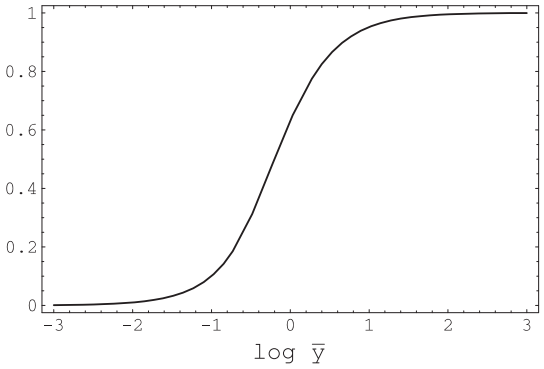

Fig. 3. Dependence of the *line* contribution, $\bar{y}[1-\exp(-1/\bar{y})]$, to the effective opacity $\chi_{\rm eff,n}(\xi;w)$ on $\bar{y}=|w|/\bar{A}$ for Poisson distributed, infinitely sharp lines of equal strength $A_0=\bar{A}$, cf. Eq. (62).

3.2.1. Specific expressions for selected line distributions

For the further evaluation of the expectation value of the radiative flux we need to specify the line strength distribution $f(A)$. We adopt a *power-law* distribution with the exponent α in the range $[A_1, A_2]$,

$$f(A)\,\mathrm{d}A=(\alpha-1)\frac{(A_1A_2)^{\alpha-1}}{A_2^{\alpha-1}-A_1^{\alpha-1}}A^{-\alpha}\,\mathrm{d}A \tag{56}$$

($\alpha\neq 1$) with $\int_{A_1}^{A_2} f(A)\mathrm{d}A=1$ and the mean line strength (Eq. (50))

$$\bar{A}=\frac{\alpha-1}{2-\alpha}\,\frac{(A_1A_2)^{\alpha-1}}{A_2^{\alpha-1}-A_1^{\alpha-1}}\left(A_2^{2-\alpha}-A_1^{2-\alpha}\right) \tag{57}$$

($\alpha\neq 2$). According to Learner (1982), a power-law with the exponent $\alpha=3/2$ is a good approximation of the distribution of a large number of "real" spectral lines; its mean line strength is $\bar{A}=\sqrt{A_1A_2}$. For further details about spectral lines distributed according to the Poisson point process we refer to Paper III.

As a power-law is a *scale-free* distribution, we can formulate the radiative expectation values in terms of $A/|w|$, i.e. express the line strengths A and $\bar{A}$ in units of the velocity gradient w (I:33). To this purpose we define

$$y=|w|/A,\quad \bar{y}=|w|/\bar{A} \tag{58}$$

and obtain with the power-law distribution (56) for Poisson distributed infinitely sharp lines

$$\left.\frac{\chi_{\rm eff,n}(\xi;w)}{\chi_{\rm eff,0}(\xi)}\right|_{\delta,\alpha}=1+\Lambda(\xi)\,\bar{y}\times\left\{\frac{\alpha-1}{y_1^{\alpha-1}-y_2^{\alpha-1}}\left[\Gamma\left(1-\alpha,\frac{1}{y_1}\right)-\Gamma\left(1-\alpha,\frac{1}{y_2}\right)\right]-1\right\} \tag{59}$$

where $\Gamma(\nu;x)=\int_x^\infty \mathrm{e}^{-t}t^{\nu-1}\mathrm{d}t$ is the incomplete gamma function. Since $\bar{y}$ is determined by α, y_1, and y_2, the ratio $\chi_{\rm eff,n}/\chi_{\rm eff,0}|_{\delta,\alpha}$ depends on the *four* parameters Λ, α, $\bar{y}$, and y_1 (or alternatively y_2).

For the particular exponent $\alpha=3/2$,

$$\left.\frac{\chi_{\rm eff,n}(\xi;w)}{\chi_{\rm eff,0}(\xi)}\right|_{\delta,3/2}=1+\Lambda(\xi)\,\sqrt{y_1y_2}\times\left\{\frac{1}{2(y_1^{1/2}-y_2^{1/2})}\left[\Gamma\left(-\frac{1}{2},\frac{1}{y_1}\right)-\Gamma\left(-\frac{1}{2},\frac{1}{y_2}\right)\right]-1\right\}. \tag{60}$$

Finally, we consider the limiting case of a power-law distribution where all lines have the *same* strength $A_0=\bar{A}$, i.e.

$$f(A)\,\mathrm{d}A=\delta(A-A_0)\,\mathrm{d}A=\delta(A-\bar{A})\,\mathrm{d}A. \tag{61}$$

For Poisson distributed infinitely sharp lines this strength distribution leads to

$$\left.\frac{\chi_{\rm eff,n}(\xi;w)}{\chi_{\rm eff,0}(\xi)}\right|_{\delta,A_0}=1+\Lambda(\xi)\cdot\bar{y}\left(1-\mathrm{e}^{-1/\bar{y}}\right). \tag{62}$$

This simple result is useful for gaining basic insight into the effect of the motions on the extinction coefficient. It depends only on the *two* parameters Λ and $\bar{y}$. The function $\bar{y}\cdot[1-\exp(-1/\bar{y})]$, shown in Fig. 3, increases monotonically from 0 to 1.

3.3. Effect of motions on the flux – examples and discussion

In this section the effect of the motions on the expectation value of the flux (or on the effective extinction) and its variation with the basic parameters is discussed upon the assumption of infinitely sharp Poisson distributed spectral lines. In order to keep the number of parameters determining $\chi_{\rm eff,n}/\chi_{\rm eff,0}$ small, we restrict ourselves to expressing the strength distribution by a *power-law* in the range $[A_1, A_2]$ with the *fixed* exponent $\alpha=3/2$ (Eq. (60)) which according to Learner (1982) is a very good empirical approximation of the distribution of "real" lines. A characteristic property of this particular power-law is that the cumulative *number* of lines $\int_{A_1}^{A} f(A)\mathrm{d}A$ varies essentially with $A^{-1/2}$, and their cumulative contribution to the *absorption*, $\int_{A_1}^{A} Af(A)\mathrm{d}A$, with $A^{+1/2}$. Hence the faint lines dominate the spectrum by number, whereas the absorption is determined by the stronger lines. We furthermore recall that for $\alpha=3/2$ the first moment of the distribution or the *mean* line strength is given by $\bar{A}=\sqrt{A_1A_2}$ (57). Taken as function e.g. of the maximum strength A_2, $\bar{A}$ can also be regarded as a measure of the relative "internal" strength distribution. For example, keeping $\bar{A}$ fixed, the contribution to the absorption by the faint lines decreases with increasing A_2 relative to that by the stronger lines. Note that the total line absorption is given by $\varrho\cdot\bar{A}$ (51).

In order to investigate how the width of the line strength distribution (i.e. the ratio A_2/A_1) influences the expectation value of the flux, we calculate $\langle\mathcal{F}(s_0,\xi;w)\rangle\,/\,\langle\mathcal{F}(s_0,\xi)\rangle$ for a fixed value of $\bar{A}$ as a function of A_2 and w. Figure 4 shows that for given w and ϱ_0 the flux increases with increasing A_2 and that the effect gets stronger for smaller line densities. Note that the static value $\langle\mathcal{F}(s_0,\xi)\rangle$ neither depends on w nor on ϱ_0. Since for increasing A_2 the relative contribution to the absorption by the lines stronger than $\bar{A}$ is reduced relative to that of the lines weaker than $\bar{A}$, the result implies that here a large number

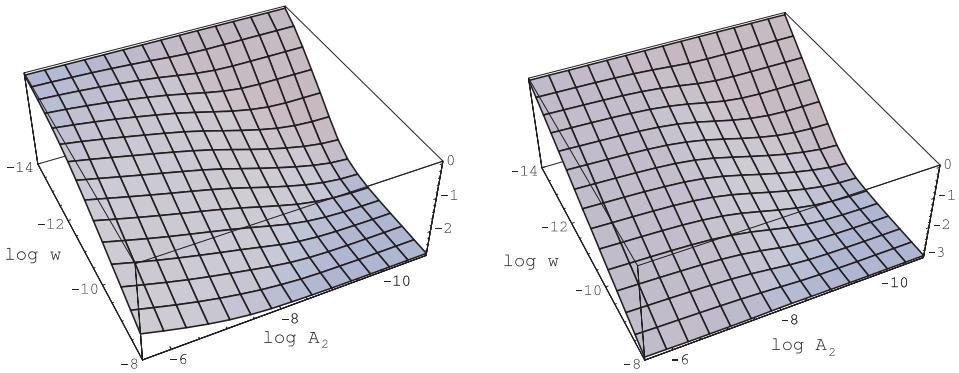

Fig. 4. $\mathrm{Log}[\langle\mathcal{F}(s_0,\xi;w)\rangle\,/\,\langle\mathcal{F}(s_0,\xi)\rangle]$ for Poisson distributed, infinitely sharp lines as function of the maximum line strength A_2 and the velocity gradient w, shown for two different line densities $\varrho_0 = 10^4$ (*left*) and 10^6 (*right*). For the line strength distribution a power-law with index $\alpha = 3/2$ (Eq. (60)) in the interval $[A_1, A_2]$ is adopted. $\chi_c = 10^{-10}$, $A_1 = 10^{-22}/A_2$.

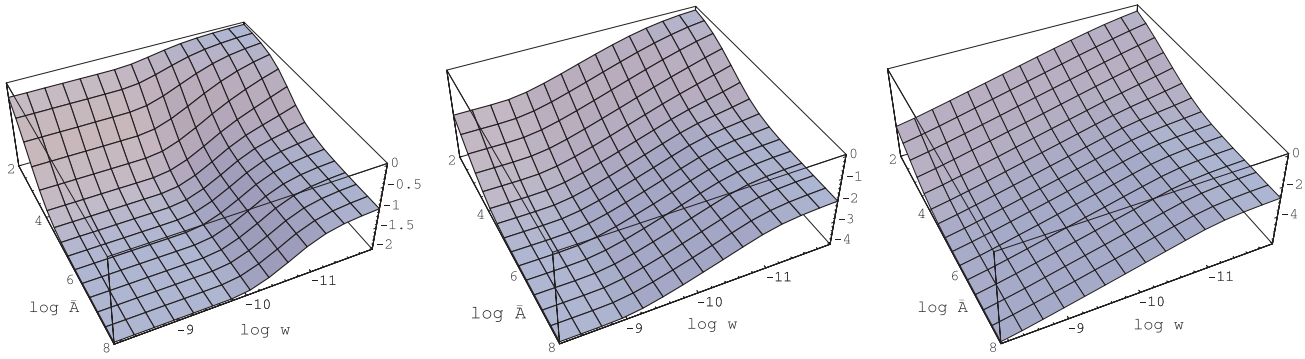

Fig. 5. $\mathrm{Log}[\langle\mathcal{F}(s_0,\xi;w)\rangle\,/\,\langle\mathcal{F}(s_0,\xi)\rangle]$ for Poisson distributed, infinitely sharp lines as function of the average line strength $\bar{A}$ and the line density ϱ_0, shown for three different velocity gradients $w = 10^{-12}$ (*left*), 10^{-10} (*middle*), and 10^{-8} (*right*). For the line strength distribution a power-law with index $\alpha = 3/2$ (Eq. (60)) in the interval $[A_1, A_2]$ is adopted. $\chi_c = 10^{-10}$, $A_2 = 10^{-8}$, $A_1 = \bar{A}^2/A_2$.

of weak lines is more effective than a small number of strong lines having the same value of $\bar{A}$.

In Fig. 5 the effect of motions on the flux is shown as a function of the line density ϱ_0 and the mean line strength $\bar{A}$. As expected, the flux is smallest for the largest values of w, ϱ_0, and $\bar{A}$. For small w, the effects of ϱ_0 and $\bar{A}$ are quite modest but highly non-linear.

It should be kept in mind that for the discussion of the dependence of the effect of the motions especially on A_2 and $\bar{A}$ the particular power-law exponent 3/2 has been assumed.

The consequences of increasing line widths for the effective opacity $\chi_{\mathrm{eff,n}}$ are depicted in Fig. 6. For this purpose, we adopt *Lorentz* profiles with different damping constants γ_0 in addition to the case with a δ-line profile. For simplicity, we furthermore assume that all Poisson distributed lines have the same strength A_0, i.e. we employ Eq. (61). Since for all curves identical values of χ_c, ϱ_0, and A_0 are used, in the limit $w \to \infty$ the same value $\chi_{\mathrm{eff,n}} = \chi_c + A_0\varrho_0$ (III:37) is reached *in*dependently of γ_0. However, for the static case the effective opacity depends strongly (up to quadratically for Lorentz profiles) on the intrinsic line width since the main part of the flux takes place between the lines and the overlapping of the lines is now controlled by γ_0. Since the flux can only decrease with increasing w (see Paper III), $\chi_{\mathrm{eff,n}}$ increases monotonically. From Fig. 6 the *total* effect of motions can be read off as the difference between the static limit (*left*) and the common limit for large velocity gradients (*right*). It is seen that the *strongest* effect occurs for the intrinsically narrowest lines, i.e. the lines with a a δ-function profile. The effect vanishes for $\gamma_0 \to \infty$, i.e. for the limiting case of a continuum.

In Table 2 – as in Fig. 6 – the dependence of the effective extinction $\chi_{\mathrm{eff,n}}$ on the line width is also demonstrated applying the same basic assumptions. The parameter combinations, however, are are chosen in a way *complementary* to those of the figure: For all examples in the table the *static* effective extinction is the *same*, namely $\chi_{\mathrm{eff},0}(\xi) \simeq 10^{-8}$. The cases chosen are "line dominated", i.e. $\varrho_0 A_0 \gg \chi_c$ or $\Lambda \gg 1$ (Eq. (51)), respectively, and the typical maximum height of a line extinction coefficient in terms of the continuum is of the order of $A_0/(\gamma_0\chi_c) \gg 1$. In all but one example $\varrho_0\gamma_0 \ll 1$ holds, i.e. the lines do not significantly overlap. For the case given in the second last line of the Table, however, $\varrho_0\gamma_0 = 1$, leading to $\chi_{\mathrm{eff,w}} \approx 10^{-8}$ *in*dependent of the velocity gradient w.

Whereas Fig. 6 shows that different static extinction coefficients may lead to identical coefficients at high velocity gradients, Table 2 demonstrates that also the *opposite* behavior can occur: identical coefficients for the static case lead to very different values at large w as can be seen from the limit $\chi_c + \varrho_0 A_0$ for large velocity gradients (cf. III:37). Therefore, there exists *no simple and universal* expression for the conversion from the static to the moving case, as e.g. for the transformation of the OP data (Seaton 1995), calculated for static media, to the conditions of supernovae or of accretion disks.

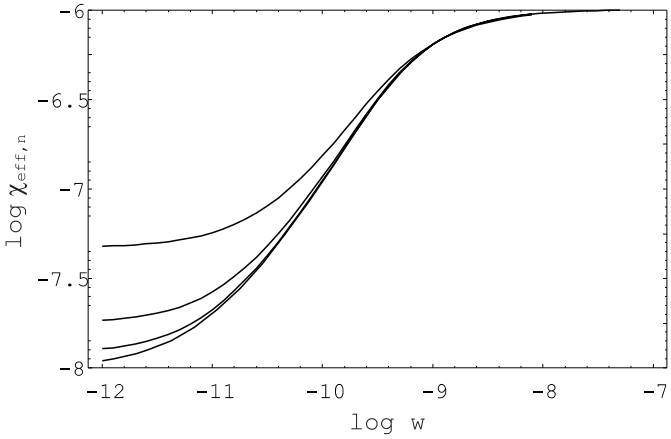

Fig. 6. Comparison of effective extinction coefficients $\chi_{\rm eff,n}(\xi; w)$ (in arbitrary units) for Poisson distributed lines of equal strength $A_0 = \bar{A}$ as function of the velocity gradient w for – *top to bottom* – Lorentz profiles with damping constants $\gamma_0 = 10^{-6}$, 10^{-5}, and 10^{-4} and one case with infinitely narrow line width.

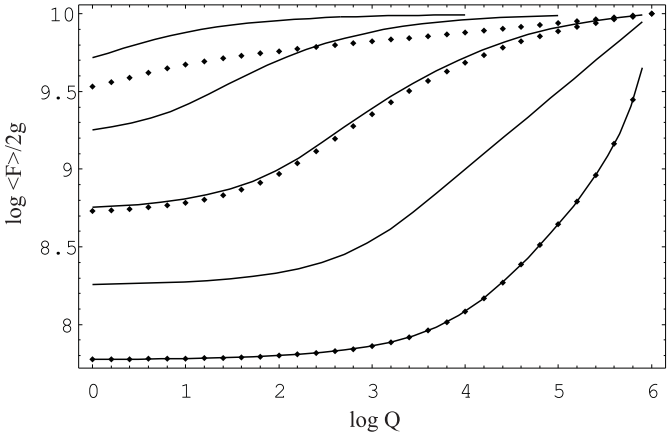

Fig. 7. $\log[\langle\mathcal{F}(s_0,\xi;w)\rangle/2g(s_0,\xi,\boldsymbol{n})] = -\log\chi_{\rm eff,n}(\xi;w)$ for Poisson distributed, infinitely sharp lines (*full curves*) with line strength distribution given by a power-law with exponent 3/2 as function of the completeness parameter Q (Eq. (63)) for velocity gradients $w = 10^{-12}$, 10^{-11}, 10^{-10}, 10^{-9}, and 10^{-8} (*top to bottom*). The additional parameters have the values $\chi_{\rm c} = 10^{-10}$, $A_1 = 10^{-12}$, $A_2 = 10^{-6}$, $\varrho_0 = 10^3$. For $w = 10^{-12}$, 10^{-10}, and 10^{-8} we plot the corresponding data also for Lorentz lines (*dotted curves*) with $\gamma_0 = 10^{-4}$ which do not strongly overlap ($\varrho_0\gamma_0 = 0.1$, cf. Sect. 3.4).

Table 2. Effective extinction in the limit of large velocity gradients, $\chi_{\rm eff,n}(\xi; w \to \infty) = \chi_{\rm c} + \varrho_0 A_0$, for Poisson distributed lines of equal strength $A_0 = \bar{A}$ with Lorentz profiles (damping constant γ_0) and δ-line profiles ($\gamma_0 \to 0$), respectively. All examples have a *common* effective extinction $\chi_{\rm eff,w}(\xi) = 10^{-8}$ at $w = 10^{-12}$ which s considered as a good approximation for the *static* case $\chi_{\rm eff,0}(\xi)$. The parameters w, $\chi_{\rm c}$, $\chi_{\rm eff}$, and A_0 have the dimension of a reciprocal length and are measured in arbitrary units; ϱ_0 and $\Lambda = \bar{A}\varrho_0/\chi_{\rm c}$ (51) are dimensionless

$\chi_{\rm c}$	ϱ_0	A_0	γ_0	Λ	$\chi_{\rm c} + \varrho_0 A_0$
4×10^{-9}	3×10^{2}	10^{-9}	10^{-4}	10^{2}	3×10^{-7}
10^{-8}	10^{3}	10^{-9}	0	10^{2}	10^{-6}
10^{-9}	10^{3}	5×10^{-9}	6×10^{-6}	5×10^{3}	5×10^{-6}
10^{-9}	10^{3}	10^{-8}	9×10^{-6}	10^{4}	10^{-5}
10^{-9}	10^{5}	10^{-13}	10^{-5}	10	10^{-8}
10^{-9}	5.8	10^{-4}	10^{-5}	6×10^{5}	6×10^{-4}

3.4. Applicability of the approximation by infinitely sharp lines

The approximation of the spectral lines by infinitely sharp profiles allowed us to derive simple expressions for the flux, elucidating in particular the effects of the motions. At this point it should be emphasized that the numerical evaluation of the effective extinction coefficients is considerably easier for infinitely sharp lines than for lines of finite width where the general, more involved expressions have to be applied. Despite these advantages the limitations of the approximation by infinitely sharp lines should be discussed.

Besides the obvious, but not too severe restriction that the lines have to be sufficiently narrow, there is a more involved problem due to the fact that δ-line profiles have no wings and do not overlap in the *static* case. On the other hand, for sufficiently large velocity gradients w the degree of overlapping is determined solely by the Doppler shifts, and the intrinsic line width is irrelevant (cf. Karp et al. 1977). This leads for *small* velocity gradients to an *overestimate* of the effect of the motions on the flux and on the effective extinction: First, Eq. (54) requires that *all* spectral lines, including the large number of faint lines, can be approximated by infinitely sharp lines. If, however, the lines have a small finite width and their total line strength $\varrho(\xi)\bar{A}$ is large, then $\chi_{\rm eff,0} > \chi_{\rm c}$, and the static reference flux is decreased correspondingly (Fig. 6). Secondly, $\chi_{\rm eff,n}/\chi_{\rm eff,0}$ can, in principle, according to Eq. (55) become arbitrarily large with increasing line density $\varrho(\xi)$ for δ-line profiles.

In a realistic situation indeed very large line densities and a strong crowding of the lines are common. For example, when modelling astronomical objects e.g. with temperatures below about 10^4 K, about 6×10^7 atomic and molecular lines in the spectral range from 10 nm to 300 μm have to be taken into account (Kurucz 1995, 1997). This corresponds to an *average* line density of 6×10^6 lines per logarithmic wavelength interval $\Delta\xi = 1$. On the other hand, assuming for a first orientation that all lines have the same spacing in ξ and the same intrinsic (natural plus thermal) width $\Delta\xi_{\rm line}$, the "just-overlapping" case $\varrho\cdot\Delta\xi_{\rm line} = 1$ is reached already for a line density of about 3×10^5 lines per $\Delta\xi = 1$ if we assume $\Delta\xi_{\rm line} = 3\times10^{-6}$ which is equivalent to a thermal velocity of about $1\,{\rm km\,s^{-1}}$. (Note that for the examples discussed in Sect. 3.3 we had for simplicity assumed that $\Delta\xi_{\rm line}$ is given solely by the damping constant γ of the Lorentz profile.) In this case the majority of lines does *not* contribute to the effective extinction *to the full extent* and hence the effect of the motions, calculated for lines with δ-line profiles for a given line density $\varrho(\xi)$ is overestimated. In such a situation, the expectation value of the flux should be calculated from the more general expressions given in Paper III which are valid for *finite* line widths.

4. Number of lines and accuracy of the flux

In the preceding section we argued that a strong crowding of spectral lines of finite width leads to a reduction of the effect

of motions on the effective extinction compared to the case of small line densities, since then parts of the lines form a quasi-continuum which is practically not affected by Doppler effects. The magnitude of the reduction increases with increasing velocity gradient w.

This section is devoted to the related problem of how many lines have to be taken into account in order to obtain – for a given w – a prescribed accuracy of the flux or the corresponding extinction, a problem which also refers to the question of the completeness of the lines at the faint end and to the problem of the accuracy of stellar atmospheres (cf. Baschek 1990).

To this purpose we choose the power-law (56) with $\alpha = 3/2$ for the line strength distribution and introduce a *completeness factor* Q in the following way: All spectral lines with strengths between A_1 and $A_1 \cdot Q$ are neglected and *not* taken into account in the calculation of the *flux* so that the expression

$$\frac{1}{2}\frac{\sqrt{A_1 A_2}}{\sqrt{A_2}-\sqrt{A_1}}\int_{A_1 Q}^{A_2} A^{-3/2}\,\mathrm{d}A \quad \text{with} \quad 1 \le Q \le A_2/A_1 \tag{63}$$

enters the calculation. $Q = 1$ describes the complete line list while the maximum value $Q = A_2/A_1$ refers to the case of no lines at all considered, i.e. to the continuum flux. For the normalization of the strength distribution, however, i.e. in the integral $\int_{A_1}^{A_2} f(A)\mathrm{d}A = 1$, the "theoretical" lower limit A_1 is to be kept.

In Fig. 7 we consider a line-dominated case ($\varrho_0 \bar{A} \gg \chi_\mathrm{c}$) plotting the diffusive flux as a function of Q for various velocity gradients: Obviously, the flux increases monotonically with Q and decreases monotonically with w (cf. Paper III). Furthermore, the fluxes for lines with finite widths are smaller than the corresponding fluxes for lines with shapes of Dirac functions; the differences, however, get very small (and therefore can hardly be recognized in the figure) for very large w. The most important result is the very different slope of the curves for large and small velocity gradients: whereas for small w the maximum sensitivity is found for small completeness factors, for large w the fluxes do not change over a wide range of Q until they increase very strongly to reach the limiting value. This implies that in case the flux has to be calculated with a given (small) error one has to be much more careful in the static case (e.g. for classical stellar atmospheres) to include as many lines as possible than in the case of large velocity gradients (e.g. for novae or accretion disks) where even the neglect of a large number of lines hardly increases the flux. A full discussion of the influences of particular parameters and an assessment of the consequences will be given in a forthcoming paper.

5. Connection of the effective opacity to the expansion opacity

Although the enhancement of the effective line absorption in expanding media had already been discussed e.g. by Castor (1970, 1974) and Castor et al. (1975) , it were Karp et al. (1977) (KLCS) – in the course of their discussion of supernova shells – who first introduced the concept of an *expansion opacity* in optically *thick* media, i.e. in the diffusion limit. Subsequently the expansion opacity has been frequently discussed and applied, e.g. by Blinnikov (1996), Eastman & Pinto (1993), and Pinto & Eastman (2000).

5.1. Connection to the observer's-frame expansion opacity of Karp et al.

According to KLCS the expansion opacity κ_exp, defined in the observer's frame, comprises the total (monochromatic) opacity at frequency ν, i.e. the sum of the continuum (Thomson scattering for application to supernovae) and of the enhanced contribution of the lines resulting from the Doppler shift. This quantity thus corresponds to our monochromatic extinction coefficient χ_n (Eq. (3)) for a deterministic line list or to $\chi_\mathrm{eff,n}$ (Eq. (53)) for Poisson distributed spectral lines. However, it should be emphasized that all our radiative quantities, including χ_n and $\chi_\mathrm{eff,n}$ are defined in the *comoving* frame which is the natural frame of thermodynamics. Nevertheless we may regard their comparison with κ_exp as meaningful because the resulting difference is irrelevant for our discussion due to the slow variation of the line density ϱ and of the transformation formulae with the wavelength or with ξ over a few line widths.

While KLCS applied a deterministic description based upon a "real" line list, we consider for the following comparison a statistical distribution of the lines in view of obtaining more general results. Furthermore we make the specific assumption that our lines are approximated by δ-functions (as did KLCS) and are distributed according to a Poisson point process (cf. Eq. (55)) so that

$$\kappa_\mathrm{exp}(\nu) \Longleftrightarrow \chi_\mathrm{eff,n}(\xi; w)\Big|_\delta \tag{64}$$

correspond to each other.

The effect of the motions (expansion) is characterized by KLCS by the (monochromatic) *enhancement factor*, defined as $\varepsilon_\nu = [\kappa_\mathrm{exp}(\nu) - \kappa_\mathrm{c}]/\kappa_\mathrm{exp}(\nu)$ with κ_c being the continuous absorption coefficient. The connection to our formalism is thus given by

$$1 - \varepsilon_\nu \Longleftrightarrow \left[\left.\frac{\chi_\mathrm{eff,n}(\xi; w)}{\chi_\mathrm{eff,0}(\xi)}\right|_\delta\right]^{-1}. \tag{65}$$

We note that the definition of ε_ν by KLCS, i.e. referring the expansion opacity to the case *without* any lines (e.g. for supernovae to Thomson scattering only) and not to the static case *including* the line absorption, may lead to misinterpretations of some of their results: the conclusion that a high density of weak lines (of finite width) can also make a large contribution to the expansion opacity is not incorrect, but this contribution is just as large in the static case.

According to KLCS the expansion opacity depends – for a line list with given line properties – on the velocity gradient only via the dimensionless *expansion parameter* "$s = \kappa_\mathrm{c}\varrho ct$" which in our nomenclature reads $\chi_\mathrm{c}/|w|$, i.e.

$$s_\mathrm{KLCS}^{-1} \Longleftrightarrow \frac{|w|}{\chi_\mathrm{c}}, \tag{66}$$

and which is of the order of $|\mathrm{d}\xi_\mathrm{D,c}|$, the Doppler shift over the mean free path of a photon in the continuum (Eq. (52)). The mean enhancement factor $\bar{\varepsilon}$ for the Rosseland opacity

vanishes in both limits $|w|/\chi_c \to 0$ and $\to \infty$; the latter limit, however, violates the condition (I:34) demanded by the diffusion approximation. The expansion opacity of KLCS can be applied only if the wavelength change $|\Delta\xi_{D,lines}|$ over one mean free path of a photon in the spectral line due to the motions is large compared to the intrinsic "local" line width $\Delta\xi_{line}$ which usually is of the order of the *thermal* Doppler width. In addition, of course, $|w|/\chi_c \ll 1$ (I:34) is required in the diffusion limit. Thus the condition

$$\Delta\xi_{line} \ll |\Delta\xi_{D,line}| < |\Delta\xi_{D,c}| \approx \frac{|w|}{\chi_c} \ll 1 \qquad (67)$$

has to be fulfilled. This case corresponds either to the limit for large w (II:3) treated in Papers II and III for lines of finite width, or to the case of infinitely sharp Dirac δ-line profiles discussed in this paper.

Recalling the result that the effect of the motions on the flux and on the effective opacity is overestimated by the approximation of δ-line profiles (Sect. 3.4), we argue that this also holds for the expansion opacity or ε_ν.

5.2. Comparison with comoving-frame expansion opacities of other authors

Since in this series we consider only the diffusion limit of radiation, we have to restrict the comparison to those formulations of expansion opacities which cover this limiting case, thus leaving out the applications to the case of optically thin continua. Furthermore we here assume stationarity of the velocity and radiation fields, non-relativistic motions, and local thermodynamic equilibrium (no scattering). Even then the complexity of the problem and consequently the diversity of the simplifying assumptions made by different authors prevents a direct, systematic comparison with the different approaches.

Note that the concepts of expansion opacity proposed so far deal only with a deterministic description of the line absorption and frequently are restricted to isolated spectral lines, whereas our approach includes also stochastic line distributions and hence is suitable to describe overlapping lines as well.

5.2.1. Expansion opacity by Höflich et al.

In their discussion of SN Ia light curve models Höflich et al. (1993) introduce an expression for the monochromatic opacity in moving media which differs from that of Karp et al. only by the addition of the continuous (bound-free and free-free) absorption coefficient to the electron scattering coefficient. Therefore the expansion opacity by Höflich et al. refers to the *observer's* frame as well, although – on the other hand – the authors use *Lagrangean* coordinates for the radiative transfer. Consequently, our remarks of Sect. 5.1 apply also here.

5.2.2. Expansion opacity by Blinnikov

Blinnikov (1996) derives a formula for the expansion opacity in moving plane-parallel and spherical media for infinitely narrow lines by means of a perturbation approach and consistently uses the comoving frame. It turns out that for a wavelength-independent continuous opacity the expression is identical to that of Karp et al. (1977) except that now – in order to obtain the expansion opacity at frequency ν – one has to sum over all lines i with frequencies $\nu_i > \nu$ (whereas following Karp et al.'s observer's-frame formulation it would be $\nu_i < \nu$).

The comoving-frame results of Blinnikov are closer to ours for the corresponding geometries than those of Karp et al.

5.2.3. Expansion opacity by Baron et al.

Baron et al. (1996) derive the comoving-frame Rosseland mean opacity κ_R^β, corresponding to our $\overline{\chi}_n(w)$, to first order of β (their Eq. (31)) from the transfer equation for spherical symmetry in the non-grey case. The derivation is based upon the assumptions of (i) a homologous flow, i.e. $w = d\beta/dr = \beta/r$, (ii) the Eddington approximation ($K_\nu = J_\nu/3$), and (iii) the equality of the monochromatic flux with the corresponding static flux in the first-moment (monochromatic) equation (their Eq. (26)).

Assumption (i), combined with considering only terms of $O(\beta)$, implies that the result is valid also only to first order of the velocity gradient w, whereas our formalism does not restrict w. Since we have shown that deterministic, symmetric and non-overlapping (II:20, 38) as well as Poisson distributed, overlapping (III:42, 45) spectral lines contribute to the generalized Rosseland opacity only to *second* order of w, the expansion opacity of Baron et al. is not expected to include the effect of lines in a moving medium.

Assumption (iii) is not consistent with our result that the monochromatic flux as well as the corresponding monochromatic opacity depends on the motions already to first order in w (cf. Eqs. (16) and (II:17)) with the wavelength-derivative of the reciprocal extinction entering the coefficient. The first-order term, integrated over wavelength, is non-zero e.g. for continua varying with wavelength while it is not important for symmetric spectral lines (see above). As a consequence of assumption (iii), also the comoving Rosseland opacity of Baron et al. (their Eqs. (30), (31)), comprising no wavelength-derivative of χ, is inconsistent with our result. This may be seen e.g. for the example of an opacity following a power-law, $\chi_\nu \propto \nu^{-n}$, given by Baron et al. and by us (Eqs. II:25, 26): For $n = 0$, i.e. for a *grey* continuum which does not depend on wavelength, they find a contribution of $2\beta/(r\chi_R^0) = 2w/\chi_R^0$ (their Eq. (34)) and a slightly different value from Eq. (29) whereas we obtain *no* effect at all of the motions.

5.2.4. Expansion opacity by Pinto & Eastman

The discussion of line opacities in expanding media by Pinto & Eastman (2000) deals on the one hand with mean values obtained by arithmetic averaging of the line extinction (cf. their Sect. 2.3) which are not comparable with our expressions which have been obtained for the diffusion limit of radiation. On the other hand, Pinto & Eastman derive also the monochromatic flux and the Rosseland opacity in the limit of large optical depths for spherically symmetric, non-relativistic flows by assuming (i) the monochromatic Eddington approximation and (ii) a thermalized radiation field, i.e. replacing the mean monochromatic intensity by the Planck

function. These expressions can directly be compared with our results and exhibit already at a first glance strong similarity in their basic structure.

In order to carry out a more detailed comparison we have to adapt our Eqs. (5) and (6) to the spherical case and a homologous velocity law: We replace s by the radial coordinate r and note that the velocity gradient w does then not depend on the direction $\boldsymbol{n}$ so that the extinction $\chi_{\rm n}(\xi; w)$ can be taken out of the integral over the solid angles ω. With $\int_{2\pi} |\boldsymbol{n}\rangle\langle\boldsymbol{n}|\,{\rm d}\omega = 2\pi/3$, we obtain for the absolute value of the *monochromatic flux* at r_0

$$F_w(r_0,\xi) = \frac{4\pi}{3}\frac{\partial T}{\partial r}\cdot\frac{\partial B(T,\xi)}{\partial T}\int_0^\infty \exp\left(-\frac{1}{w}\int_{\xi-wr}^{\xi}\chi(\zeta){\rm d}\zeta\right){\rm d}r. \tag{68}$$

On the other hand, Eq. (21) of Pinto & Eastman has also to be modified in order to facilitate the comparison: ct is identified with w^{-1}, the signs of spatial coordinates and gradients are adapted, and the frequency scale ν is replaced by our logarithmic wavelength scale $\xi = \ln\lambda = -\ln\nu$ so that ${\rm d}\xi = -{\rm d}\nu/\nu$, ${\rm d}\xi' = -{\rm d}\nu'/\nu'$, and ${\rm d}\zeta = -{\rm d}\nu''/\nu''$. The Planck function $B_\nu(T)$ and the flux F_ν are transformed to $B(T,\xi)$ and $F_w^{\rm PE}(r_0,\xi)$, respectively, which refer to a unit wavelength interval. Finally, $\varrho\kappa_\nu$ is written as $\chi(\xi)$ yielding

$$\begin{aligned} F_w^{\rm PE}(r_0,\xi) &= \frac{4\pi}{3}\frac{\partial T}{\partial r}\int_{-\infty}^{\xi}\frac{\partial B(T,\xi')}{\partial T}{\rm e}^{-3(\xi-\xi')}\exp\left(-\frac{1}{w}\int_{\xi'}^{\xi}\chi(\zeta){\rm d}\zeta\right)\frac{{\rm d}\xi'}{w} \\ &= \frac{4\pi}{3}\frac{\partial T}{\partial r}\int_0^\infty\frac{\partial B(T,\xi-wr)}{\partial T}{\rm e}^{-3wr}\exp\left(-\frac{1}{w}\int_{\xi-wr}^{\xi}\chi(\zeta){\rm d}\zeta\right){\rm d}r, \end{aligned} \tag{69}$$

where the second expression has been obtained by substituting $\xi'-\xi = -wr$.

The *Rosseland mean* opacity $\chi_{\rm n}(\xi; w)$ (or $\kappa_{\rm R}$ in Pinto & Eastman's notation) is then defined in either case by the relation

$$\chi_{\rm n}(\xi; w)^{-1} = \frac{3}{4\pi}\left[\frac{\partial T}{\partial r}\,B(T)\right]^{-1}\int_{-\infty}^{\infty}F_w(r_0,\xi)\,{\rm e}^{\xi}\,{\rm d}\xi, \tag{70}$$

where n here refers to the radial direction. (Note that there is a typographical error in Eq. (23) of Pinto & Eastman: instead of $\kappa_{\rm R}$ read $\kappa_{\rm R}^{-1}$.)

Comparing our expression $F_w(r_0,\xi)$ for the flux in homologously expanding spheres with the corresponding $F_w^{\rm PE}(r_0,\xi)$ of Pinto & Eastman we first note the essential similarity for this geometry and this velocity field. The formulae differ (i) by the factor $\exp(-3wr)$ which does not occur in our expression and is of minor importance since the main contribution to the integral comes from the vicinity of $r = 0$, and (ii) in that we have assumed $\partial B(T,\xi)/\partial T$ to be a sufficiently slowly varying function that can be taken out of the integral over wavelength.

In conclusion of the discussion of various expansion opacities we note that the expressions given by Karp et al. (1977), Blinnikov (1996), and Pinto & Eastman (2000) are suitable to calculate numerically the modification of the effective opacity due to motions. They correspond to our Eq. (I:39), but are written in a way that is not favorable to physical insights (as e.g. for the contribution of lines) and the derivation of interesting general properties. The formulae of Karp et al. and Blinnikov are restricted to large velocity gradients ("Sobolev approximation") due to the assumption of infinitely narrow intrinsic lines profiles.

In this series we have in addition considered our expressions with a *stochastic* model for the line absorption that allows us for the first time not only to estimate e.g. the influence of different line types and of line overlap, but also to tremendously reduce the number of input data.

6. Conclusions and outlook

In this series about radiation in the diffusion limit the radiative flux has been derived and the classical concept of the Rosseland opacity been generalized to slowly differentially moving 3D media. The presentation of the spectral lines by a stochastic distribution based on a Poisson point process turned out very flexible and allowed us to obtain closed expressions of the radiative quantities as well as general insight into the effect of the motions on them.

In this last paper of the series first the flux *vector* has been derived for a general velocity field in which the velocity gradient $w(\boldsymbol{n})$ depends on the direction $\boldsymbol{n}$, i.e. in which the corresponding extinction coefficient is a tensor. As steps on the way to deriving the flux vector various different types of flux and their associated extinction coefficients have been introduced for deterministic as well as for stochastic line extinction. In the deterministic case we have to distinguish the following monochromatic and wavelength-integrated extinction coefficients: (i) for a static or uniformly moving medium χ_0 and $\bar{\chi}_0$ where the latter is identical to the Rosseland mean opacity $\bar{\chi}_{\rm R}$, (ii) the "directional" extinctions $\chi_{\rm n}$ and $\bar{\chi}_{\rm n}$ which refer to the fluxes in direction $\boldsymbol{n}$ (with velocity gradient w), and (iii) the extinction *tensors* $\boldsymbol{X}_\beta$ and $\bar{\boldsymbol{X}}_\beta$ for the flux vector. For the stochastic description there are six analogous *effective* extinction coefficients associated with the expectation values of the fluxes.

In the static case the flux depends on the direction only via the projection of the temperature gradient and therefore the angle integrations can easily be performed. For fluxes in moving media in *general* due to the additional dependence on $\boldsymbol{n}$ via w, no further analytical simplifications seem possible.

In the special case of *small* w, however, we can obtain closed expressions that allow important new insights, in particular, on the properties of the flow and on the deviation of the flux vector from the direction of the temperature gradient. Furthermore, it is seen directly, that in moving media the flux vector is made up by the static value and products of (scalar) terms, which depend on the physics of the radiating species only, and (tensor) terms which depend on derivatives of the velocity field only.

The multiple integrals in the expressions of the flux for Poisson distributed lines for the case of small velocity gradients have in general to be calculated numerically where the integral over $\hat{\xi}$ in fact requires particular attention, whereas the ξ-integral is fast since $\varrho(\hat{\xi},\vartheta)$ is a slowly varying function of wavelength. However, the integrals do not depend on the

Table A.1. Relationships between monochromatic and total radiation fluxes in the diffusion approximation and their corresponding equivalent opacities.

monochromatic		
flux in direction $\boldsymbol{n}$	$\mathcal{F}(s_0,\xi;w) = 2\,\frac{\partial B(T,\xi)}{\partial T}\,\left[\chi_{\rm n}(\xi;w)\right]^{-1}\,\boldsymbol{n}\cdot\nabla T$	Eq. (3)
	$\left\langle\mathcal{F}(s_0,\xi;w)\right\rangle = 2\,\frac{\partial B(T,\xi)}{\partial T}\left[\chi_{\rm eff,n}(\xi;w)\right]^{-1}\boldsymbol{n}\cdot\nabla T$	(29)
– , *static*	$\mathcal{F}(s_0,\xi) = 2\,\frac{\partial B(T,\xi)}{\partial T}\,\left[\chi_0(\xi)\right]^{-1}\,\boldsymbol{n}\cdot\nabla T$	see text
	$\left\langle\mathcal{F}(s_0,\xi)\right\rangle = 2\,\frac{\partial B(T,\xi)}{\partial T}\left[\chi_{\rm eff,0}(\xi)\right]^{-1}\boldsymbol{n}\cdot\nabla T$	(31)
flux vector	$\boldsymbol{F}_w(s_0,\xi) = \frac{4\pi}{3}\,\frac{\partial B(T,\xi)}{\partial T}\,\left[\boldsymbol{X}_\beta(\xi)\right]^{-1}\,\nabla T$	(6)
	$\left\langle\boldsymbol{F}_w(s_0,\xi)\right\rangle = \frac{4\pi}{3}\,\frac{\partial B(T,\xi)}{\partial T}\left[\boldsymbol{X}_{\rm eff,\beta}(\xi)\right]^{-1}\nabla T$	(6)
– , *static*	$\boldsymbol{F}(s_0,\xi) = \frac{4\pi}{3}\,\frac{\partial B(T,\xi)}{\partial T}\,\left[\chi_0(\xi)\right]^{-1}\,\nabla T$	see text
	$\left\langle\boldsymbol{F}(s_0,\xi)\right\rangle = \frac{4\pi}{3}\,\frac{\partial B(T,\xi)}{\partial T}\left[\chi_{\rm eff,0}(\xi)\right]^{-1}\nabla T$	(31)
wavelength-integrated		
flux in direction $\boldsymbol{n}$	$\mathcal{F}_{\rm tot}(s_0;w) = 2\,\frac{\partial B(T)}{\partial T}\,\left[\bar{\chi}_{\rm n}(w)\right]^{-1}\,\boldsymbol{n}\cdot\nabla T$	Eq. (9)
	$\left\langle\mathcal{F}_{\rm tot}(s_0;w)\right\rangle = 2\,\frac{\partial B(T)}{\partial T}\left[\bar{\chi}_{\rm eff,n}(w)\right]^{-1}\boldsymbol{n}\cdot\nabla T$	(35)
– , *static*	$\mathcal{F}_{\rm tot}(s_0) = 2\,\frac{\partial B(T)}{\partial T}\,\left[\bar{\chi}_{\rm R}\right]^{-1}\,\boldsymbol{n}\cdot\nabla T$	(15)
	$\left\langle\mathcal{F}_{\rm tot}(s_0)\right\rangle = 2\,\frac{\partial B(T)}{\partial T}\left[\bar{\chi}_{\rm eff,0}\right]^{-1}\boldsymbol{n}\cdot\nabla T$	(37)
flux vector	$\boldsymbol{F}_{{\rm tot},w}(s_0) = \frac{4\pi}{3}\,\frac{\partial B(T)}{\partial T}\,\left[\bar{\boldsymbol{X}}_\beta\right]^{-1}\,\nabla T$	(12)
	$\left\langle\boldsymbol{F}_{{\rm tot},w}(s_0)\right\rangle = \frac{4\pi}{3}\,\frac{\partial B(T)}{\partial T}\left[\bar{\boldsymbol{X}}_{\rm eff,\beta}\right]^{-1}\nabla T$	(36)
– , *static*	$\boldsymbol{F}_{\rm tot}(s_0) = \frac{4\pi}{3}\,\frac{\partial B(T)}{\partial T}\,\left[\bar{\chi}_{\rm R}\right]^{-1}\,\nabla T$	(15)
	$\left\langle\boldsymbol{F}_{\rm tot}(s_0)\right\rangle = \frac{4\pi}{3}\,\frac{\partial B(T)}{\partial T}\left[\bar{\chi}_{\rm eff,0}\right]^{-1}\nabla T$	(37)

velocity field and therefore can be calculated once for all. The cost for the proper inclusion of velocity fields is therefore only about twice the cost for the static case.

Our results are valid for essentially all types of differentiable profile functions. Lines profiles of interest that do not fall into this class are triangular, box shape and infinitely narrow profiles. In fact, for these profiles several of the above integrals can be performed analytically and therefore allow a very fast evaluation, but the expansions for small velocity gradients require special attention.

For Poisson distributed *Dirac δ-lines* – which can be described by a minimum set of parameters – we have explicitly evaluated the expectation value of the radiative flux upon the assumption that the line strengths are given by a power-law and applied it to discuss the basic effects of the motions on the flux. In particular we have given a first assessment of the dependence of the accuracy of the flux calculation on the completeness of the spectral line list for different velocity gradients.

The comparison of the observer's-frame expansion opacity introduced by Karp et al. with our more general comoving-frame effective extinction coefficients shows that the expansion opacity is related to $\chi_{\rm n}$ or $\chi_{\rm eff,n}$, respectively.

Aspects yet to be worked out for the treatment of spectral lines by means of the Poisson point process include

(i) an assessment of the accuracy of this approach. Although first checks (Wehrse et al. 1998) indicate that the assumptions of our stochastic process are well fulfilled, a covariance function has still to be calculated to have an estimate of the inherent stochastic error;

(ii) an explicit treatment of scattering processes. This would be of particular interest also for optically thin parts of a configuration;

(iii) a discussion of the radiative energy balance based upon the divergence of the vector of the total flux;

(iv) the derivation of the vector of the radiative acceleration and pressure tensor for moving media, of further moments of the specific intensity, and of the Eddington approximation;

(v) the connection of the flux vector and effective extinction to the corresponding formulation in terms of generalized opacity distribution functions (Baschek et al. 2001) for lines distributed according to a Poisson point process;

(vi) the actual calculations of effective mean opacities for a large grid of temperatures, densities and chemical compositions; and last but not least

(vii) the application to specific astronomical objects and problems.

Acknowledgements. We are indebted to Chr. Graf and G. Shaviv for many stimulating discussions. This work has been supported in part by the DFG (Sonderforschungsbereich 359/C2).

Appendix A: Fluxes and associated opacities

In Table A.1 are listed the relationships between the various types of radiation flux in the diffusion approximation and their

associated equivalent opacities. The expressions for the flux are first given for spectral lines of a *deterministic* sample, followed by its expectation value (denoted by acute parentheses) for lines with a *stochastic* distribution. All quantities refer to the spatial position s_0, but note that in the notation for the temperature T and its gradient ∇T, for all opacities χ, $\bar{\chi}$, $\boldsymbol{X}$, and $\bar{\boldsymbol{X}}$ and for the velocity gradient $w = w(\boldsymbol{n})$ the variable s_0 has been suppressed in order to keep the notation relatively simple.

The last column of the Table contains references to the equations of this paper which are relevant to the various types of extinction coefficients. $\chi_0(\xi)$ is the "normal" (isotropic) extinction coefficient comprising the continuum χ_c and the contribution $X(\xi) = \sum_l \chi_l(\xi)$ of L lines.

References

Baschek, B. 1990, in Atomic spectra and oscillator strengths for astrophysics and fusion research, ed. J. E. Hansen (Koninkl. Akad. van Wetenschappen, Verhandl. Afd. Natuurk., Eerste Reeks 33 North Holland, Amsterdam), 33

Baschek, B., von Waldenfels, W., & Wehrse, R. 2001, A&A, 371, 1084

Baron, E., Hauschildt, P. H., & Mezzacappa, A. 1996, MNRAS, 278, 763

Blinnikov, S. I. 1996, Astron. Lett., 22, 79 [Pis'ma v AZh, 22, 92]

Castor, J. I. 1970, MNRAS, 149, 111

Castor, J. I. 1974, MNRAS, 169, 279

Castor, J. I., Abbott, D. C., & Klein, R. I. 1975, ApJ, 195, 157

Cohen-Tanoudji, C., Diu, B., & Laloë, F. 1977, Quantum mechanics, vol. I (New York: John Wiley)

Eastman, R. G., & Pinto, P. A. 1993, ApJ, 412, 731

Fichtenholz, G. M. 1973, Differential- und Integralrechnung I (VEB Deutscher Verlag der Wissenschaften, Berlin), 267

Höflich, P., Müller, E., & Khokhlov, A. 1993, A&A, 268, 570

Karp, A. H., Lasher, G., Chan, K. L., & Salpeter, E. E. 1977, ApJ, 214, 161 (KLCS)

Kurucz, R. L. 1995, An atomic and molecular data bank for stellar spectroscopy, in Laboratory and astronomical high resolution spectra, ed. A. J. Sauval, R. Blomme, & N. Grevesse, Astron. Soc. Pacific Conf. Ser., 81, 17

Kurucz, R. L. 1997, Progress on model atmospheres and line data, in Proc. First ISO Workshop on Astrophysical Spectroscopy, Madrid, ESA SP-419, 193

Learner, R. C. M. 1982, J. Phys. B, 15, L891

Pinto, P. A., & Eastman, R. G. 2000, ApJ, 530, 757

Seaton, M. J. 1995, The opacity project, vol. 1, compiled by the Opacity Project Team (Bristol: Inst. Physics Publ.)

Wehrse, R., Baschek, B., & von Waldenfels, W. 2000a, A&A, 359, 780 (Paper I)

Wehrse, R., Baschek, B., & von Waldenfels, W. 2000b, A&A, 359, 788, Paper II

Wehrse, R., Baschek, B., & von Waldenfels, W. 2002, A&A, 390, 1141, Paper III

Wehrse, R., von Waldenfels, W., & Baschek, B. 1998, JQSRT, 60, 963

Weil, H. 1966, Classical groups (Princeton University Press, 8th printing 1973)